Chromogenic mechanisms in blue-and-white porcelains

Ariane Pinto, Jesse Groenen, Bing Zhao, Tiequan Zhu, Philippe Sciau

HAL Id: hal-03491479
https://hal.science/hal-03491479

Submitted on 22 Aug 2022

Chromogenic mechanisms in blue-and-white porcelains

Ariane PINTO[a*1], Jesse GROENEN[a], Bing ZHAO[c], Tiequan ZHU[def], Philippe SCIAU[a*]

[a] CEMES, Université de Toulouse, CNRS, 29 rue Jeanne Marvig, 31055, Toulouse, France

[b] CRCAO UMR 8155, CNRS, 52 Rue du Cardinal Lemoine, 75005 Paris, France

[c] School of Sociology and Anthropology of Sun Yat-sen University, 135 Xigangxi Road, Guangzhou 510275, China

[d] Southern Marine Science and Engineering Guangdong Laboratory (Zhuhai) Zhuhai, 519000, China

[e] The Joint Research Center of Maritime Silk Road by Sun Yat-sen University and Yangjiang Municipal Government, Yangjiang, 529500, China

* Corresponding authors: ariane.pinto@cea.fr; philippe.sciau@cemes.fr

Abstract

The blue underglaze decorations of Chinese blue-and-white porcelains are due to the use of a cobalt-based blue pigment. Nevertheless, for a same time period and production centre, wares can present wide colour variations in both hue and intensity. Fourteen Ming samples were investigated using colorimetry, Raman spectroscopy and SEM-EDS, in order to better understand the origin of these variations. The majority of the sherds dates back to the middle 15th- early 16th century. The chromogenic mechanism of the hue and intensity variations appears to be complex and multifactorial. Six main factors have been identified: the elemental composition of the pigment particles, in particular the Fe/Co ratio, the pigment spinel structure, the size as well as the distribution of the colouring particles, the environment of the pigment particles and the colour of the glaze.

Keywords

Chinese porcelains; Blue pigment; Spinel; Cobalt aluminate; Raman spectroscopy

Introduction

Blue colour holds a special dimension in many civilisations for its association with calm, peace or natural environments such as sky or water [1]. Natural blue colouring agents are also very rare. Blue colour was mostly obtained from expensive Lapis-Lazuli or cobalt oxides, or produced as a synthetic pigment from copper minerals (e.g. Egyptian blue) [2]. In the case of Chinese blue-and-white porcelain, famous around the world for the finesse of its blue decorations contrasting with the white body, a cobalt-based pigment was applied on the ware before glazing. After one-step firing at high temperature (1250-1300°C), it resulted in underglaze blue decorations [3]. Blue-and-white porcelain manufacturing process is well mastered since the Yuan Dynasty (1279-1368 AD) and the production

---

[1] Present adress : Arc Nucléart, CEA Grenoble, 17 avenue des Martyrs, 38054 GRENOBLE Cedex 9

become massive under the Ming Dynasty (1368-1644 AD) [3]. However, productions from the same time period and production centre show blue decorations with significant colour variations both in hue (vivid blue to greenish blue) and intensity (dark to light blue) (**Fig. 1**).
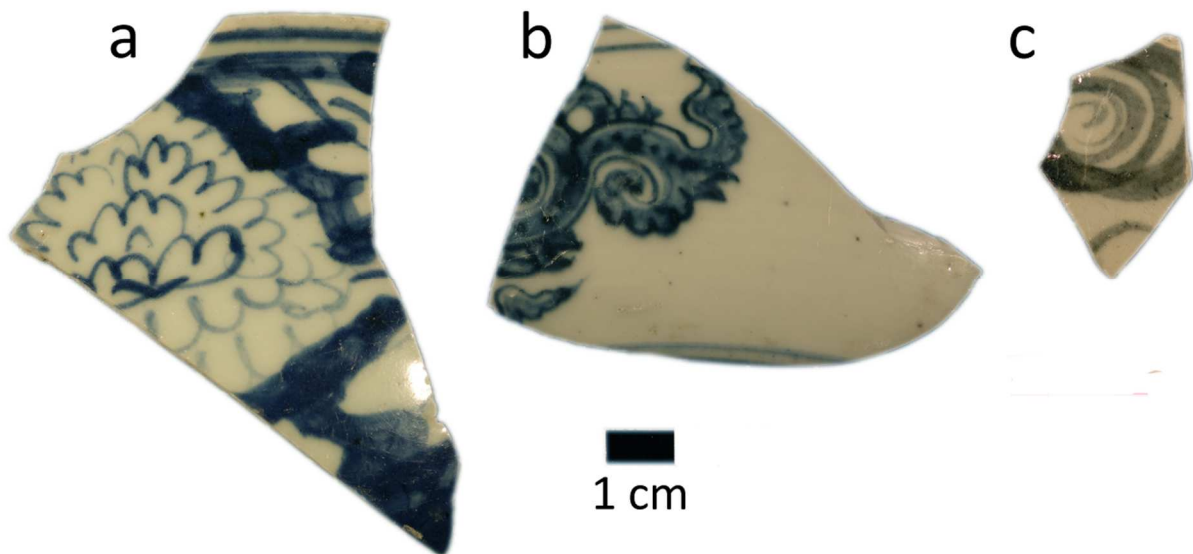
Figure 1 : Different blue decoration hues on Ming samples. (a) Sample TZ09: vivid blue. (b) Sample TZ06: greenish blue. (c) Sample TZ07: grey.

Numerous researches have been dedicated to the chromogenic mechanisms at the origin of these colour variations [4]. For a long time, the chemical composition of the pigment and the concentration of transition elements (Co, Fe, Mn) were considered main parameters in the hue variation [5-10]. In their study on Yuan Dynasty productions (1279-1368 AD), Tiequan ZHU *et al.* [9] correlated the colour variation to Co/Fe and Co/Mn ratios. On Ming Dynasty productions (1368-1644 AD), light blue and dark blue show different Mn/Co and Fe/Co ratios, dark blue zones being richer in Mn with respect to iron [6-7].

Different studies on the pigment zone showed the presence of Co-based phases, including $CoAl_2O_4$ and CoO [11-14]. They have a direct impact on the blue colour, but their connection with the hue variation was not clearly established [4]. Furthermore, some studies highlighted the presence of acicular crystals of anorthite ($CaAl_2Si_2O_8$) surrounding the Co-based phases and mentioned a potential role in the chromogenic process [13,15]. Finally, on the surface of the glaze, the formation of Fe and Mn-rich phases (Fe_2O_3, Fe_3O_4, Mn_3O_4) are also responsible for the darkening of the blue decorations [16].

In most of the previous studies, the composition of cobalt pigment and the Co-based phases were identified through the glaze. Its thickness inevitably induces a loss of information regarding the size, concentration and distribution of pigment underglaze crystals [4]. Therefore, previous studies can be contradictory due to the complexity of the pigment zone and its inaccessibility. In this study, we took advantage of a corpus of fourteen samples produced during the Ming Dynasty, between the middle of the 15th and early 17th century. We combine two approaches. Firstly, we performed colorimetric measurements at the surface of the samples. Secondly, we carried out elementary and microstructural analysis on cross-sections cut at the exact location of the surface measurements. Then, we were able to connect the colour seen by the naked eye to the underglaze microstructure and to uncover crucial parameters explaining the shade variation.

Samples and method

2.1 Samples description and preparation

All the studied samples have been excavated from the urban site of Maojiawang (Xichengqu district, Beijing municipality). This pit of 8.3 meters long and 5.6 meters wide, excavated in 2005, has yielded more than 100,000 fragments of ceramics originated from 20 kilns sites in China [17]. According to stylistic study, the fourteen samples studied were produced at Jingdezhen and surrounding area (Jiangxi Province). They can be dated from the middle and late Ming Dynasty (middle 15th-early 17th century) and the majority of sherds is dated from the middle 15th-early 16th century. They were provided by the Beijing Archaeological Institute through Pr. Tiequan Zhu (Archaeometry Lab, Sun Yat-Sen University, Guangzhou). Descriptions and illustrations of samples are presented in **Appendices** (**A.1** and **Table A.2**).

In order to obtain objective data to compare the different blue variations we used colorimetry. Measurements were carried out on the surface of the wares and yielded different colour groups. Among these groups, nine representative samples (TZ05, TZ07, TZ08, TZ09, TZ10, TZ12, TZ16, TZ19, TZ20) were selected and cut on the exact location of the colorimetric measurements to gain access to the underglaze microstructure. The other five sherds were not cut because of the size of the fragments and the place of the colorimetry measurements. Sampling would have been too damaging for the sherds. The obtained cuts were mounted in epoxy resin and polished to obtain clean cross-sections.

2.2 Colorimetry

Colours of blue and white zones were measured on the surface of the wares using a Konica Minolta CM-700d spectrometer with a 10° angle. For each measurement, data for specular components included (SCI) and excluded (SCE) were taken simultaneously. We used a 3 mm aperture to adapt to small zones. Each zone underwent 3 to 5 measurements. Mean value of measurements are presented in **Appendices** (**Table A.3**). The colorimetric data was exploited using the CIELab 1976 system. Each colour is defined by three values: a* expresses the green (-100) and red (+100) components, b* the blue (-100) and yellow (+100) components and L* the brightness between black (0) and white (100).

2.3 Micro-Raman spectrometry

Micro-Raman spectrometry was performed on cross-sections at room temperature using a Xplora MV 2000 Horiba spectrometer with a solid-state laser excited at 532 nm; this single grating set-up equipped with an edge filter to eliminate elastic scattering has a high optical throughput, enabling high sensitivity with short acquisition times. The spectrometer is equipped with 100× microscope objectives, confocal set-ups and charge coupled device detectors.

2.4 Scanning electron microscopy

The electron microscopy investigations were performed on cross-sections using a scanning electron microscope (JEOL JSM 6490) equipped with an energy-dispersive X-ray spectrometer (SEM-EDS)

3

109 (IncaPentaFet X3). Both imaging and elemental analyses were performed in HV (*high vacuum*) mode,
110 working distance 10 mm. The imaging was performed in backscattered electron mode. The electron
111 acceleration was 15 kV for imaging and elemental analysis. Since ceramics are not conductive, a thin
112 layer of carbon covered the cross-sections, in order to avoid any charging effect during the
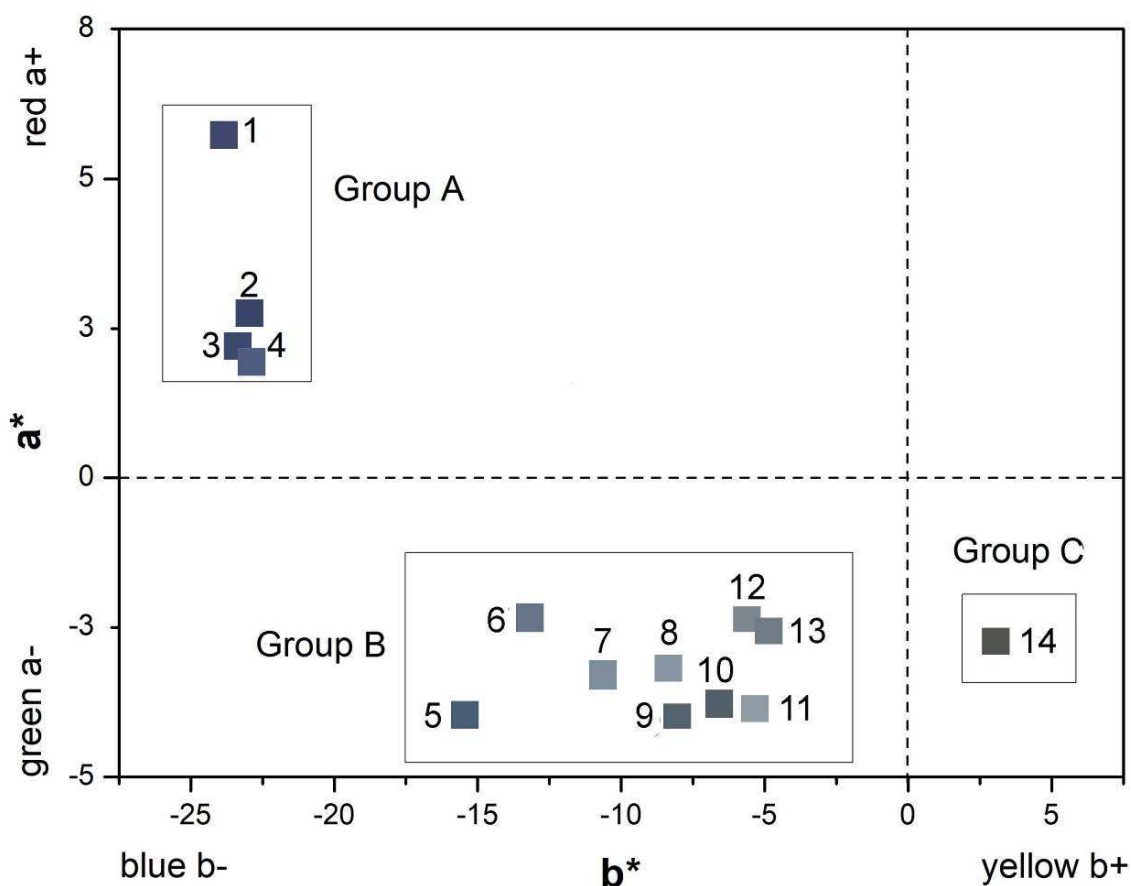113 measurements.

Results

3.1 Colorimetry

119
120 **Figure 2 : Chromatic diagram of blue decorations**. Only a* and b* values are showed. The colour
121 corresponding to L*a*b* values are reported at the location of each point.
122 Group A: (1) TZ08; (2) TZ09; (3) TZ10; (4) TZ11;
123 Group B: (5) TZ21; (6) TZ14; (7) TZ12; (8) TZ16; (9) TZ05; (10) TZ06; (11) TZ19; (12) TZ20; (13) TZ13,
124 Group C: (14) TZ07.

126 The colorimetric measurements on blue decorations are presented in **Appendices** (**Table A.3)** and
127 synthesized in **Fig. 2**. Based on the a* and b* values, we defined three groups. *Group A* includes four
128 samples (TZ08, TZ09, TZ10, TZ11). The colorimetric values are characterized by a negative b* and a
129 positive a* value corresponding to a vivid slightly purplish blue. This group contains the more vivid
130 blue samples with a b* value below -21. *Group B* includes nine samples (TZ05, TZ06, TZ12, TZ13,

4

131 TZ14, TZ16, TZ19, TZ20, TZ21). The colorimetric values are characterized by negative a* and b* values
132 corresponding to a dull slightly greenish blue. *Group C* is constituted of a single sample (TZ07) with a
133 negative a* and a positive b* value. The blue decoration appears grey.

134 The colorimetric measurements on the white zones, without decorations, are presented in
135 **Appendices** (**Table A.3)** and synthesised in **Fig. 3**. The transparent glaze is not perfectly colourless.
136 The a* and b* values point to a yellow-greenish colour.
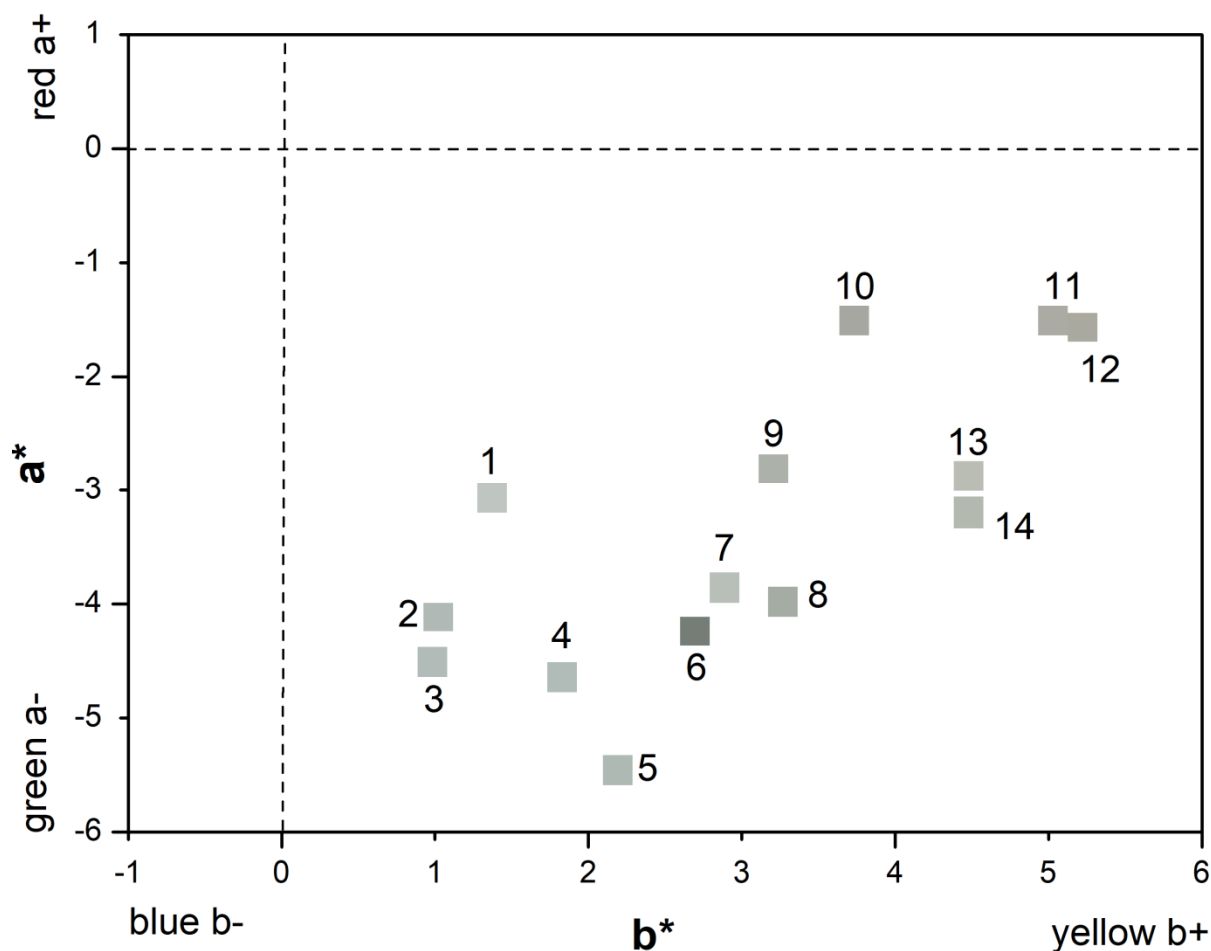
137
138 **Figure 3 :** Chromatic diagram of white zones. Only a* and b* values are showed. The colour corresponding to
139 L*a*b* values are reported at the location of each point. (1) TZ10; (2) TZ09; (3) TZ11; (4) TZ19; (5) TZ20; (6)
140 TZ08; (7) TZ12; (8) TZ13; (9) TZ14; (10) TZ07; (11) TZ06; (12) TZ05; (13) TZ16; (14) TZ21.

141

3.2 Observations

143 Pigment zone observations, performed on cross-sections, show similar microstructure with both
144 crystalline and amorphous phases. On **Fig. 4a** the bright pigment particles are surrounded by a thick
145 layer of acicular crystals. This type of microstructure was already spotted in multiple studies on blue-
146 and-white porcelains dated from the Ming Dynasty [13,15].

147 **Fig. 4b** shows examples of a blue decoration zone presenting no pigment particle. The glaze is
148 directly in contact with the body, but the pigment zone appears, in chemical contrast, lighter than
149 the glaze indicating a different chemical composition. This different composition is most likely due to
150 high concentration of transitional elements (Mn, Fe, Co) resulting from the pigment dissolution in the

5

151 glaze. Previous studies showed the possible absence of a specific zone containing pigment particles
152 and anorthite crystals between the glaze and the body, where transition elements have completely
153 diffused into the glaze [4,11]. In these cases, Co^{2+} ions react in tetrahedral coordination with the
154 glaze network, leading to a blue colour. However, due to its lower tinting contribution, the density of
155 color is lower [4]. Wang *et al*. also indicate that Fe ions in the glaze have no significant role in the
156 color and Mn ions can have an influence on the darkening rather than on the hue [4].
157
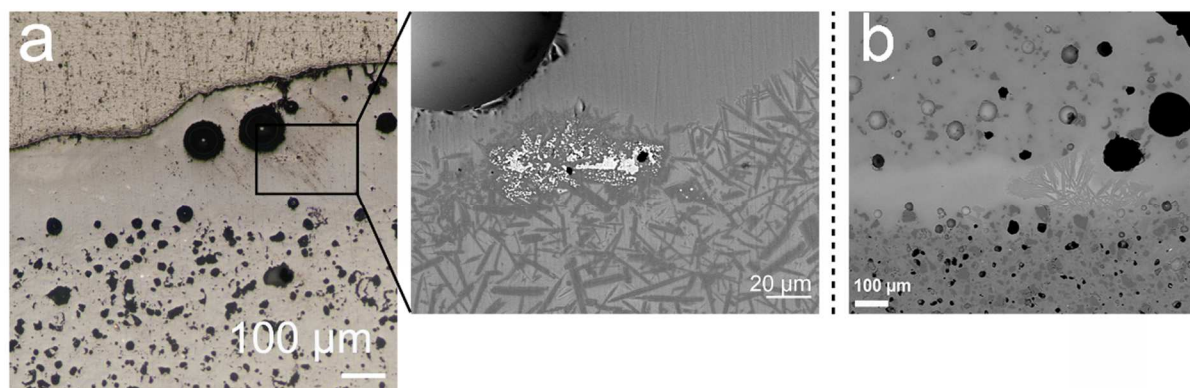
159 **Figure 4 : Microstructures of the pigment zones.** (a) With crystalline structures (optical and SEM images),
160 sample TZ02; (b) Without pigment particle (SEM images), sample TZ20.

161

162 ### 3.3 Micro-Raman spectrometry

163 Bright pigment particles and acicular crystals were investigated using micro-Raman spectrometry.
164 Raman spectrum measured on pigment particles are displayed in **Fig. 5**. Spectra are characterized by
165 six peaks, with positions and relative intensities that are consistent with the Raman spectrum of
166 cubic spinels, more precisely aluminates with the general formula AAl_2O_4 [18]. The partially inverse
167 structure of some aluminates ($CoAl_2O_4$, $FeAl_2O_4$, $MnAl_2O_4$, $MgAl_2O_4$) can cause the activation of
168 additional Raman modes, in particular a second A_{1g} mode between 699 et 720 cm^{-1} noted as A_{1g}*
169 [18].

170 **Fig. 5** shows three groups of spectra. *Group 1* spectra are defined by large and less pronounced peaks
171 dominated by an A_{1g} mode, between 739 and 763 cm^{-1}. They can be discriminated by a small $F_{2g}(1)$
172 mode. *Group 2* spectra are similar to *Group 3* spectra, with a dominant A_{1g} mode between 748-
173 754 cm^{-1}, but they can be discriminated by an A_{1g}* mode distinct from the main A_{1g} mode and a $F_{2g}(1)$
174 mode more intense. *Group 3* spectra are similar to *Group 2* spectra because of an intense $F_{2g}(1)$
175 mode, as the dominant mode, but the $F_{2g}(2)$ and A_{1g} modes have the same intensity and are more
176 intense than $F_{2g}(3)$ mode. From the modes' relative intensity and positions, *Group 1* spectra are close
177 to hercynite ($FeAl_2O_4$) references [18-19]. *Group 2* spectra have an intense $F_{2g}(1)$ mode, more
178 characteristic of galaxite ($MnAl_2O_4$) and cobalt aluminate ($CoAl_2O_4$) [14,18,20]. The relative intensity
179 of *Group 3* spectra Raman modes is close to $MnAl_2O_4$, but the positions of $F_{2g}(1)$, E_g, $F_{2g}(2)$ and A_{1g}
180 modes are closer to those reported for $CoAl_2O_4$ [18,20].
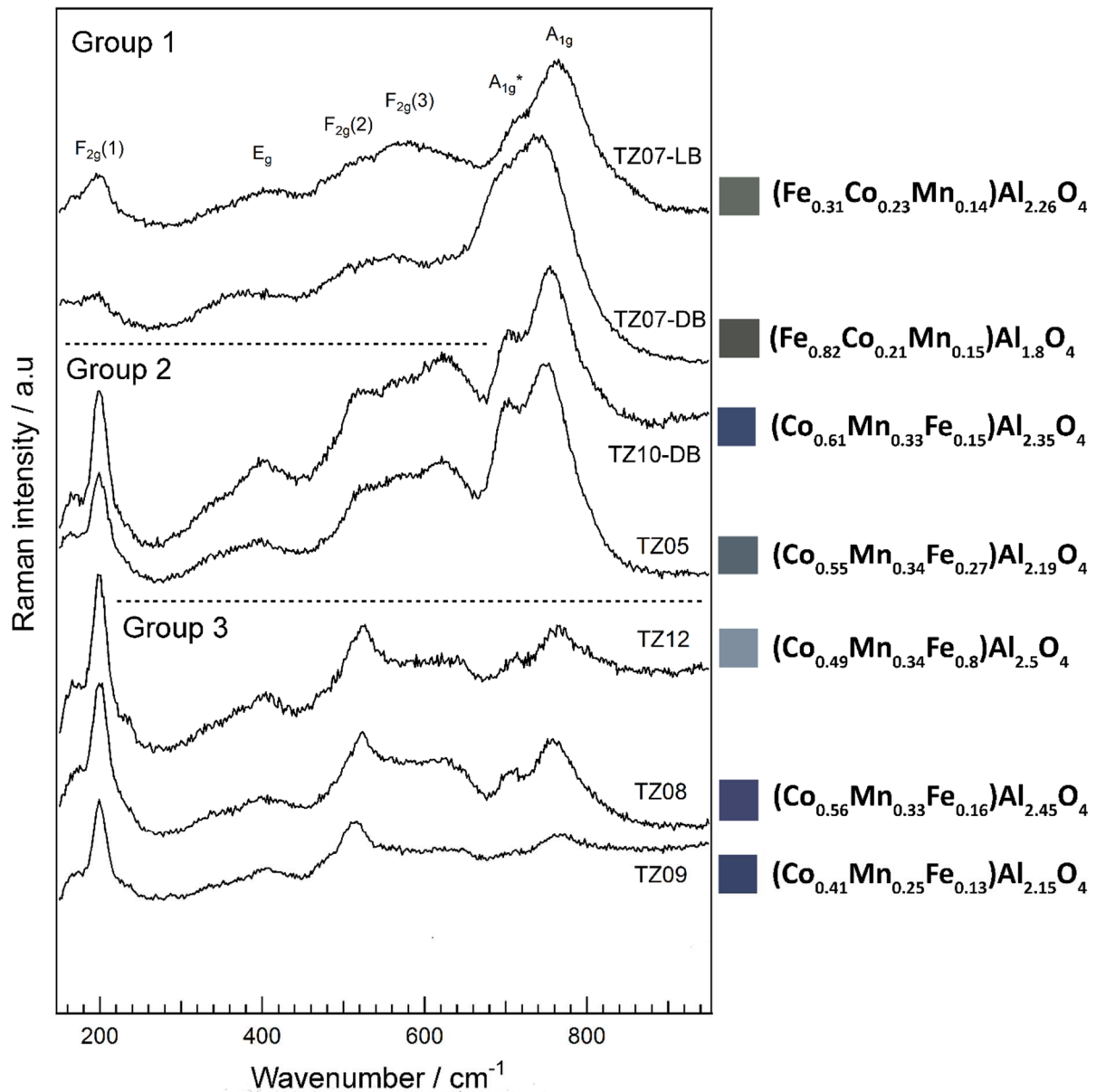
Figure 5 : Raman spectra measured on pigment particles. For each Raman spectrum, we also indicate the chemical formula calculated from the SEM-EDS point measured on the same location and the surface colour measured by colorimetry. DB for Dark Blue and LB for Light Blue zones.

Acicular crystals were identified as anorthite ($CaAl_2Si_2O_8$) from their Raman spectra thank to the dominant double peak at 479 and 506 cm^{-1}, and four less intense peaks at 191, 278, 406 et 561 cm^{-1} [21] (spectra shown in **Appendice Fig. A.4**).

3.4 SEM-EDS

The different types of aluminates are hard to distinguish from their Raman spectra because the differences in the E_g, $F_{2g}(2)$ and A_{1g} wavenumbers do not exceed 3-4% [18]. SEM-EDS provided the chemical composition at the same spot as the micro-Raman spectrometry analysis. All the points studied are illustrated in **Appendix A.5.** The complete chemical compositions are presented in **Appendices (Table A.6)**. From these compositions we calculated a formula based on aluminates

195 structure (AAl$_2$O$_4$), where A can be Co, Fe and Mn. The calculated chemical formulas corresponding
196 to each Raman spectrum are outlined on **Fig. 5**.

197 Although micro-Raman spectrometry distinguished three groups, calculated chemical formulas are
198 only of two types: a composition closer to hercynite (FeAl$_2$O$_4$) with Co and Mn substitution (TZ07),
199 and a chemical composition close to cobalt aluminate (CoAl$_2$O$_4$) with more or less Mn and Fe
200 substitutions (TZ05, TZ08, TZ09, TZ10, TZ12). The presence of cobalt aluminate (CoAl$_2$O$_4$) as a blue
201 pigment in blue-and-white porcelains was widely reported these two last decades [7,13-14,22-26].

202 Chemical substitutions (Mn, Fe, Co, Ni, Mg) are due to the existence of solid-solutions between
203 CoAl$_2$O$_4$, FeAl$_2$O$_4$ and MnAl$_2$O$_4$. Co^{2+}, Fe^{2+} and Mn^{2+} mostly adopt tetrahedral coordination, which
204 eases the substitutions. Mg can also be present as substitutions and sample TZ16 even shows a high
205 Mg content, superior to cobalt (see **Table A.6**). TZ16 pigment particles belong to the solid-solution
206 between CoAl$_2$O$_4$ and MgAl$_2$O$_4$, with the gradual substitution of Co^{2+} ions by Mg^{2+} ions on tetrahedral
207 sites [27].

208

209

210 ## Discussion

211

212 ### 4.1 Pigment chemical composition

213 The blue colour in blue-and-white porcelains is due to the use of cobalt. Co-rich minerals can cause
214 blue colour when they are dissolved in siliceous glass, but other transition elements (Fe, Mn etc.) can
215 also affect the final hue. **Table 1** shows the content of colouring elements (Mn, Fe, Co) in pigment
216 grain depending on the L*, a* and b* parameters measured on the surface. The content of colouring
217 elements was measured by SEM-EDS and is expressed in atomic percent (at%). Detailed compositions
218 of pigment particles are presented in **Appendices** (**Table A.6**).

219 TZ08, TZ09 and TZ10 samples are characterised by a high cobalt content. They are also part of the
220 colour *Group A* with a negative b* parameter (-22.98 > b* > -23.96) correlated to a vivid blue.
221 However, TZ05 (*Group B*) also shows a high cobalt rate, but the b* parameter indicates a less vivid
222 blue and the a* parameter a greenish colour. Thus, the amount of cobalt is not the only parameter
223 inducing the vividness of the blue.

224 The iron content also influences the vividness of the blue. *Group A* samples, with vivid blue
225 decorations, also show low Fe/Co ratio (<0.30). The higher the Fe/Co ratio is, the higher the b*
226 parameter is, causing a less vivid blue. A similar trend is observed in Vietnamese porcelains, where
227 iron was probably added to modify the blue decoration from a vivid blue to a greenish one [5]. TZ07
228 (*Group C* sample) shows a high amount of iron (11.87 at%). It has a strong impact on the colour since
229 this sample is the only one showing a positive b* parameter and a grey colour.

230 The manganese content does not appear to have any direct impact on the blue colour variation. Mn^{3+}
231 ions in glass can produce a purple colour while Mn^{2+} is colourless. However, samples with a*
232 parameter, connected to a slightly purplish colour, are not the ones with the higher Mn content or
233 the ones with the higher Mn/Co ratio. Due to mainly reducing firing conditions, manganese is
234 probably mostly in Mn^{2+} explaining its absence of impact on colour.

Colour Group	ID	Composition						Colorimetry		
		Co	Mn	Fe	Fe/Co	Mn/Co	Mn/Fe	L^*	a^*	b^*
	TZ08	7.30	4.23	2.02	0.28	0.58	2.09	30.5	5.76	-23.96
A	TZ10-DB	8.16	4.35	1.96	0.24	0.53	2.22	31.37	2.24	-23.47
	TZ09	5.65	3.36	1.71	0.30	0.59	1.96	29.55	2.77	-22.98
	TZ16	4.71	2.57	1.71	0.36	0.55	1.50	61.78	-3.20	-8.35
B	TZ05	7.24	4.54	3.55	0.49	0.63	1.28	41.4	-3.99	-8.09
	TZ20	5.29	4.75	2.73	0.52	0.90	1.74	55.94	-2.37	-5.76
	TZ19	3.24	2.07	3.48	1.07	0.64	0.59	63.98	-3.84	-5.45
C	TZ07-DB	2.93	2.02	11.87	4.05	0.69	0.17	35.4	-2.66	3.18

Table 1 : Transition elements content (at%) in pigment particles and colorimetric measurements. The colour groups presented in Fig. 2 are also mentioned.

4.2 Pigment structure

The chromogenic mechanism of blue coloration is due not only to the type and relative amount of transition elements in the pigment. The oxidation state of metallic ions (valence) and the stereochemistry (coordination) are also key parameters.

As seen in the chemical formula shown in **Table A.6**, TZ02, TZ05, TZ08, TZ09, TZ10, TZ12 and TZ20's pigment particles have composition close to cobalt aluminate ($CoAl_2O_4$) but with Mn and Fe substitutions. Cobalt aluminate, also called 'cobalt blue', presents a vivid blue colour resulting from tetrahedral Co^{2+} electronic transitions leading to the characteristic absorption band at 550-680 nm [20,28-31]. Tetrahedral coordination of Co^{2+} ions is key to obtain an intense blue colour [32]. This was observed on TZ08, TZ09, TZ10 and TZ12. On **Fig. 5**, the Raman spectra show an intense $F_{2g}(1)$ mode which has been ascribed to the Co-O stretching vibration in tetrahedral coordination [20]. This proper coordination is obtained through a high synthesis temperature, typically between 1000°C and 1200°C [33]. The vivid blue colour of TZ08, TZ09 and TZ10 appears to be connected to substituted $CoAl_2O_4$ particles obtained at high firing temperature, with Co^{2+} in proper tetrahedral coordination.

However, numerous studies showed that $CoAl_2O_4$ colour depends largely on its composition, structure and annealing temperature [34-37]. For the same chemical composition, $CoAl_2O_4$ can show blue or green colour depending on structural disorder connected to the synthesis temperature [36-37]. According to Shiva Salem and Federica Bondioli [37], the green coloration is due to a partially inverse spinel structure, obtained at low temperature, where part of Co^{2+} ions occupy octahedral sites. In contrast, the vivid blue colour is the result of a normal spinel structure, synthesized at high temperature, with Co^{2+} on tetrahedral sites. On the Raman spectrum presented in their study, the 516 cm^{-1} peak is very intense for the blue $CoAl_2O_4$ and less visible for the green $CoAl_2O_4$. TZ05's Raman spectrum (**Fig. 5**) shows a less visible 516 cm^{-1} peak and an additional A_{1g}^* mode attributed to spinel inversion [18]. Its greenish colour could then be explained by pigment grain with an inverse spinel structure and Co^{2+} ions on octahedral sites.

9

264 Sample TZ07 exhibits a grey colour due to the presence of hercynite ($FeAl_2O_4$) substituted with Mn
265 and Co. This phase gives rise to a dark colour [38] explaining the unusual hue of the « blue »
266 decoration. Hercynite formation in TZ07 is connected to the high amount of Fe in the pigment
267 particles and the firing under reducing conditions.

268 Sample TZ16 exhibits a light blue and a unique composition of the pigment in the $MgAl_2O_4$-$CoAl_2O_4$
269 solid solution with Mn and Fe substitutions. Numerous studies have explored pigments with
270 compositions in the $Co_xMg_{1-x}Al_2O_4$ solid solution [27,31,35,39-40]. It appears that Mg-substituted
271 $CoAl_2O_4$ colour varies from light blue to dark blue with the increase of Co with respect to Mg [31,39].
272 In TZ16, the light blue colour could then be linked to a high amount of Mg (equal to Co) (**Table A.6**).

273

4.3 Size and distributions of particles

275 The pigment zones show different size and distribution of pigment particles. On SEM images, we
276 selected an area of 100 x 75 μm and we performed a particle counting using Image J software
277 (**Appendice A.7**). A threshold range is set to discriminate the objects of interest from the
278 background, in particular the pigments particles from the glassy matrix and the acicular crystals.
279 Eight samples were analysed (TZ08, TZ09, TZ10, TZ16, TZ19, TZ20). **Table A.8** shows the number of
280 particles on the analysed zone, the average size of particles and the number of particles depending
281 on their size.

282 In Tian WANG *et al*. [4], it appears that the number of cobalt aluminate particles influences the blue
283 intensity, with dark blue decorations containing higher number of particles than light blue zones. In
284 our case, the total number of particles measured on a 100 x 75 μm area ranges from 140 (TZ16) to
285 894 (TZ10). Samples presenting the more vivid blue ($-22.98 > b^* > -23.96$) reveal a pigment zone with
286 a high number of particles (TZ08, TZ09, TZ10). Likewise, some of the samples with the lightest blue
287 decoration ($-5.45 > b^* > -8.35$) show a pigment zone with a small number of particles (TZ16, TZ19,
288 TZ05). However, this tendency is not systematic since TZ20 show a high number of particles (475) but
289 a b^* value characteristic of a lighter blue ($b^* = -5.76$). Others parameters such as the environment of
290 the colouring particles can explain this exception.

291 The average size of particles also plays a key role in the chromogenic process concerning both the
292 hue and the colour intensity. The two samples with the more vivid blue (TZ08 and TZ10) show
293 pigment zones with high particle average size (0.840 and 0.795 μm²). For TZ08, some pigment
294 particles can even reach 50 μm². In contrast, pigment particle average size, in TZ16, TZ19, and TZ20
295 with less intense blue, do not exceed 0.305 μm². Similar observations can be made concerning the
296 colour intensity defined by the L^* value. **Fig. 6** shows the correlation between the L^* value and the
297 average size of particles. Except from TZ09, the lesser the average size of particles is, the higher is the
298 L^* value and lighter the colour. Nevertheless, TZ09 belongs to *Group A*, with the darker and more
299 vivid blue hues, thanks to the amount of cobalt and the coordination of the $CoAl_2O_4$ spinel, as we
300 have seen above.
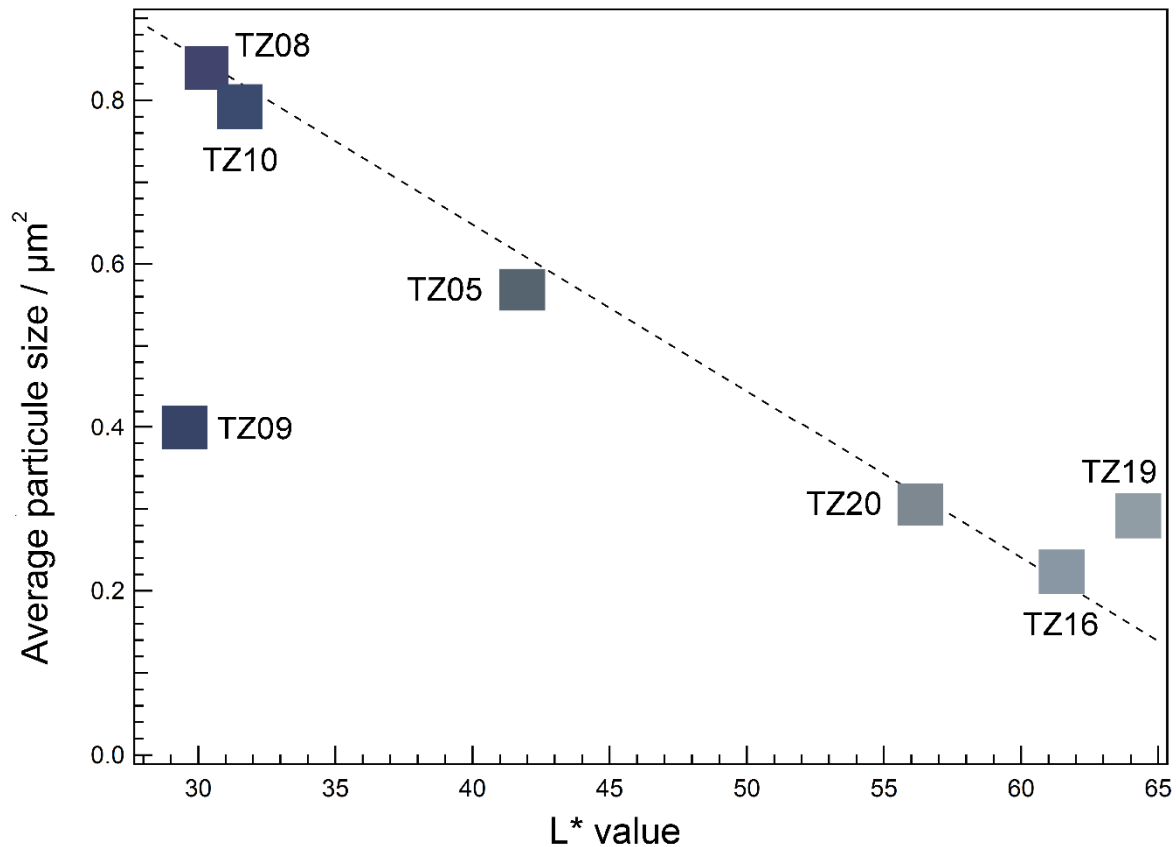
Figure 6 : Average particles size (µm²) in function of L* value (luminosity). The surface colour measured by colorimetry is also indicated.

4.4 Pigment particles environment

Ming samples pigment zones are also characterised by the presence of acicular crystals of anorthite surrounding the pigment particles. Several studies show a connexion between the density of anorthite crystals and the vividness of the blue [4,15]. According to Xiaochenyang Jiang *et al.* [15], the development of anorthite crystals during firing tends to act as a barrier coating to hinder the further dissolution of pigment particle and diffusion of cobalt ions. To verify if a thick anorthite layer is connected to a vivid blue, we studied eight pigment zones on seven samples (TZ05, TZ08, TZ09, TZ10-DB dark blue, TZ10-LB light blue, TZ16, TZ19, TZ20). **Fig. 7** shows the different pigment zones with three main tendencies.

Upper line samples (**Fig. 7a-b-c-d**) show the more vivid blue colours (22.98 < b*< - 23.96 for TZ08, TZ09, and TZ10-DB), as well as TZ05, which is greenish. All samples present a similar pigment zone with a thick layer (around the hundreds of microns) of acicular anorthite crystals surrounding the pigment particles. The glassy matrix between the anorthite crystals is lighter than the rest of the glaze, indicating that transition elements have diffused from the pigment particles. The upper line samples also include the darkest blue samples (29.55 < L*< 41.4). *A contrario,* the lower line (**Fig. 7e-f-g-h**) shows samples with the lightest blue (55 < L* < 62 for TZ16; TZ20, TZ10 LB, TZ19) characterized by the absence of a thick and homogeneous layer of anorthite crystals. TZ16 and TZ20 (**Fig. 7e-f**) present a "jumble" of anorthite crystals surrounding small pigment particles and no acicular crystals

can be seen for TZ10-LB and TZ19 (**Fig. 7g-h**). Thus, a dark and vivid blue colour is directly connected to a dense and thick layer of anorthite crystals.
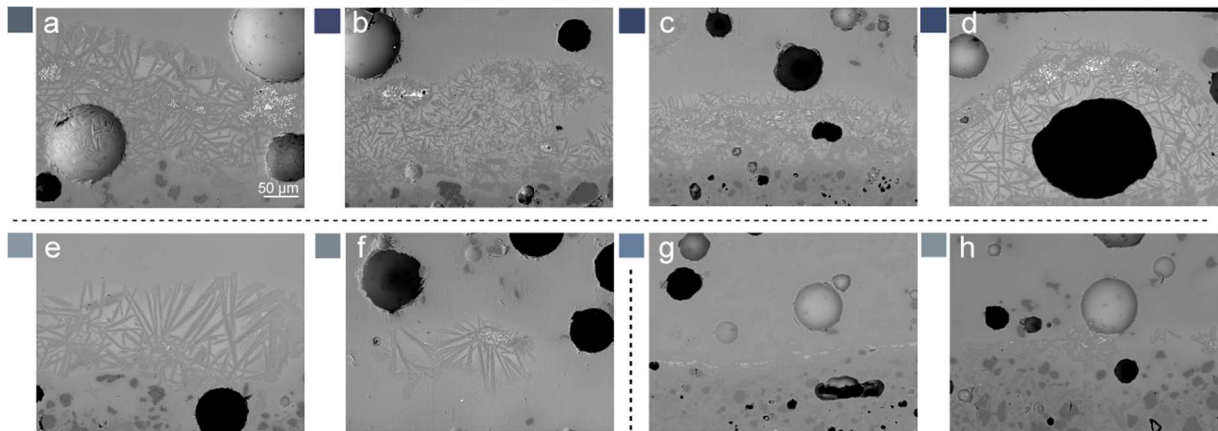
Figure 7 : Electronic images of pigment zones with crystalline structures. Polished cross-sections observed in BSE mode. The surface colours, measured by colorimetry, are also indicated. (a) TZ05; (b) TZ08; (c) TZ09; (d) TZ10-DB; (e) TZ16; (f) TZ20; (g) TZ10-LB; (h) TZ19.

Furthermore, sample TZ20 also exhibits blue decoration zones although no pigment particles are observed, as showed previously on **Fig. 4b**. Corresponding colorimetric measurements indicate a dull and light blue. In this case, the lack of intensity in the blue colour is more likely due to a partial dissolution of the pigment in the glassy matrix with the diffusion of the Co^{2+} ions above 900°C [41]. Similar phenomenon may have occurred for the lower line samples (**Fig. 7e-f-g-h**). The presence of a thin anorthite layer or no anorthite at all, allowed a partial dissolution of the pigment in the glassy matrix leading to small particle sizes and light and dull blue colours.

4.5 Glaze contribution

The white zone colorimetric analysis (**Fig. 3, Table A.3**) showed that glaze is not colourless. It can be slightly tinted in green-yellow or green-blue due to the presence of iron in ionic form. In glasses, Fe^{2+} gives a pale blue colour, whereas Fe^{3+} gives a yellow one [42]. Additional colours (amber, green-blue, brown) can be obtained with different Fe^{2+}/Fe^{3+} ratios [43]. Iron was not intentionally added as a colouring element, since blue-and-white porcelain used a colourless and translucent glaze, but it was present in the raw material. Because the glaze is put on the pigment, its coloration has an impact on the final blue coloration. It can reduce the vividness of the blue and create a greenish shade.

4.6 Summary

Samples from *Group A* present the more vivid and darker blue (b* > -22.98) and they all show the same pigment zone microstructure: numerous large pigment particles (average size > 0.4 µm²) comprised of cobalt aluminate ($CoAl_2O_4$) with lightly substituted with iron, surrounded by a thick layer of acicular anorthite crystals preventing their dissolution in the glassy matrix. TZ09 exhibits the lowest density of pigment grain and smallest average size, but the high cobalt content, the tetrahedral Co^{2+} coordination and the thick anorthite layer maintain a vivid blue colour.

354 Samples from *Group B* are characterized by a dull, greenish and lighter blue, but this colour hue may
355 result from a wide variety of parameters. Not aiming to review group B, we exemplify this variety
356 considering some representative samples:

357 - TZ05 has many parameters in common with *Group A* samples, such as the presence of
358 $CoAl_2O_4$-type crystals, the size and number of colouring particles and the pigment zone
359 microstructure with a thick anorthite layer. Nevertheless, pigment particles show a higher
360 Fe/Co ratio than *Group A* samples and $CoAl_2O_4$ likely show an inverse spinel structure with
361 Co^{2+} ions on the octahedral sites. In this case, the composition and structure of pigment
362 particles lead to a greenish colour rather than a vivid blue one.

363 - TZ16 differs from other samples because of a singular pigment composition with a high
364 amount of magnesium, leading to a light and dull blue colour.

365 - For TZ19 and TZ20, the light and dull blue colour is mainly attributed to small pigment
366 particles and the lack of a thick layer of acicular anorthite crystals.

367 Finally, sample TZ07's grey (*Group C*) decorations are due to a high amount of iron in the pigment
368 particles leading to the formation of hercynite ($FeAl_2O_4$) under the reducing conditions of firing.

369 The different parameters do not have the same impact on the colour. For instance, in the presence of
370 large and numerous particles of cobalt aluminate, the colour of the glaze will not have a strong
371 influence on the final colour. It will result in vivid dark blue decorations even if the glaze if coloured
372 by Fe ions.

373

374

Conclusion

376 Combining surface colorimetric measurements and cross-section analysis using micro-Raman
377 spectrometry and SEM-EDS proves to be truly insightful. We have shown that quantitative data
378 and correlations can be assessed to identify the most relevant parameters involved in chromogenic
379 mechanisms in blue-and-white porcelains. Multiple factors impact the blue colour variation with a
380 complex interplay between parameters such as the chemical and structural composition of the
381 pigment, the size and distribution of pigment particles, their environment and the glaze colour. In
382 addition, our analysis provides information relevant to technical processes used in order to design
383 the blue-and-white porcelain decorations.

384 From a technical perspective, obtaining a dark and vivid blue colour requires a pigment zone
385 microstructure containing numerous large crystals of weakly substituted cobalt-aluminate,
386 surrounded by a thick layer of acicular anorthite crystals. In order to achieve that, Chinese potters
387 needed to master the purification and the high-temperature formation of the cobalt aluminate as
388 well as insure the formation of the anorthite layer. For instance, insufficient purification of the cobalt
389 preparation would lead to the formation of cobalt aluminate crystals strongly substituted with iron,
390 or even dark-grey hercynite crystals in the most iron-rich environments.

391 From a historical point of view, the wide variation in blue colour cannot be correlated to any time
392 period within the Middle and Late Ming Dynasty (middle 15th- early 17th century). The manufacturing
393 process does not seem to undergo any significant change. A wide range of blue colour was therefore

obtained under different reigns through chemical and microstructural variations. These subtle shades of blue give this famous porcelain production its authentic charm.

Bibliography

[1] Pastoureau M. Blue: the History of a Color. Princeton: Princeton University Press, 2001.

[2] Zucchiati A, Bouquillon A, Katona I., D'Alessandro A. The 'Della Robbia blue': a case study for the use of cobalt pigments in ceramics during the Italian Renaissance. Archaeometry 2006; 48: 131-152. https://doi.org/10.1111/j.1475-4754.2006.00247.x

[3] Li Z, Bower VL , Li H. Chinese Ceramics: From the Paleolithic Period through the Qing Dynasty (The Culture & Civilization of China). New Heaven: Yale University Press, 2010.

[4] Wang T, Zhu T, Feng Y, Fayard B, Pouyet E, Cotte M, De Nolf W, Salomé M, Sciau, P. Synchrotron radiation-based multi-analytical approach for studying underglaze color: The microstructure of Chinese Qinghua blue decors (Ming dynasty). Anal Chim Acta 2016*;* 928: 20-31. https://doi.org/10.1016/j.aca.2016.04.053

[5] Colomban P, Sagon G, Huy L, Liem N, Mazerolles, L. Vietnamese (15th century) blue-and-white, Tam Thai and lustre porcelains/stonewares: glaze composition and decoration techniques. Archaeometry 2004*;* 46: 125-136. https://doi.org/10.1111/j.1475-4754.2004.00148.x

[6] Wen R, Wang C, Mao Z, Huang Y, Pollard A. The chemical composition of blue pigment on Chinese blue-and-white porcelain of the Yuan and Ming. Archaeometry 2007; 49: 101-115. https://doi.org/10.1111/j.1475-4754.2007.00290.x

[7] Coutinho M, Muralha V, Mirão J, Veiga J. Non-destructive characterization of oriental porcelain glazes and blue underglaze pigments using μ-EDXRF, μ-Raman and VP-SEM. Appl Phys A 2014, 114: 695-703. https://doi.org/10.1007/s00339-013-8147-8

[8] Simsek G, Colomban P, Wong S, Zhao B, Rougeulle A, Liem N. Toward a fast non-destructive identification of pottery: The sourcing of 14th-16th century Vietnameseand Chinese ceramic shards. J Cult Herit 2015; 16: 159-172. https://doi.org/0.1016/j.culher.2014.03.003

[9] Zhu T, Ding X, Kusimba C, Feng, Z. Using laser ablation inductively coupled plasma mass spectroscopy (LA-ICP-MS) to determine the provenance of the cobalt pigment of Qinghua porcelain

433   from Jingdezhen in Yuan Dynasty of China (1271-1368 AD). Ceram Int 2015, 41: 9878-9884.
434   https://doi.org/doi:10.1016/j.ceramint.2015.04.064

435   [10] Zhu T, Zhang Y, Xiong H, Feng Z, Li Q, Cao B. Comparison of the Different Types of Qinghua
436   Porcelain from Jingdezhen in the Yuan Dynasty of China (1271-1368 AD) by Micro X-ray Fluorescence
437   Spectroscopy (μ-XRF) and Microscopy. Archaeometry 2016; 58: 966-978.
438   https://doi.org/doi:10.1111/arcm.12215

439   [11] Wang L, Wang C.S. Co speciation in blue decorations of blue-and-white porcelains from
440   Jingdezhen kiln by using XAFS spectroscopy. J Anal At Spectrom 2011; 26: 1796-1801.
441   https://doi.org/10.1039/c0ja00240b

442   [12] Figueiredo M, Silva T, Veiga J. A XANES study of cobalt speciation state in blue-and-white glazes
443   from 16th to 17th century Chinese porcelains. J Electron Spectroscop 2012; 185: 97-102.
444   https://doi.org/10.1016/j.elspec.2012.02.2007

445   [13] Qu X, Xu J, Xi X, Huang C, Yang J. Microstructure characteristics of blue-and-white porcelain from
446   the folk kiln of Ming and Qing Dynasties. Ceram Int 2014; 40: 8783-8790.
447   https://doi.org/10.1016/j.ceramint.2014.01.100

448   [14] Kock L, De Waal D. Raman studies of the underglaze blue pigment on ceramic artefacts of the
449   Ming dynasty and of unknown origins. J Raman Spectrosc 2007; 38: 1480-1487.
450   https://doi.org/10.1002/jrs.1805

451   [15] Jiang X, Ma Y, Chen Y, Li Y, Ma Q, Zhang Z, Wang C, Yang Y. Raman analysis of cobalt blue
452   pigment in blue and white porcelain. A reassessment. Spectroc Acta A 2018; 190: 61-67.
453   https://doi.org/10.1016/j.saa.2017.08.0767

454   [16] Wu J, Li J, Guo J. Microstructure study of color spots of Jingdezhen blue and white porcelain. J
455   Inorg Mater 1999; 14: 143-149.

456   [17] Beijing wenwu yanjiusuo. Excavation Report on a Ming Period Burial at Maojiawan. Beijing:
457   Kexue chubanshe; 2007.

458   [18] D'Ippolito V, Andreozzi G, Bersani D, Lottici P. Raman fingerprint of chromate aluminate and
459   ferrite spinels. J Raman Spectrosc 2015; 46: 1255-1264. https://doi.org/10.1002/jrs.4764

460   [19] Ospitali F, Sabeta T, Tullini F, Nannetti M, Di Lonardo G. The role of Raman microspectroscopy in
461   the study of black gloss coatings on Roman pottery. J Raman Spectrosc 2005; 36: 18-23.
462   https://doi.org/10.1002/jrs.1259

463   [20] Bouchard M, Gambardella A. Raman microscopy study of synthetic cobalt blue spinel used in the
464   field of art. J Raman Spectrosc 2010; 41: 1477-1485. https://doi.org/10.1002/jrs.2645

465   [21] Sarma S, Simons B, Joder HJ. Raman study of anorthite, calcium Tschermak's pyroxene, and
466   gehlenite in crystalline and glassy states. Am Mineral 1983; 68: 1113-1125.

467   [22] De Waal D. Raman investigation of ceramics from 16th and 17th century Portuguese shipwrecks. J
468   Raman Spectrosc 2004; 35: 346-349. https://doi.org/10.1002/jrs.1210

469   [23] De Waal D. Raman analysis of underglaze pigments on porcelain art. J Raman Spectrosc 2007;
470   38: 956-957. https://doi.org/10.1002/jrs.1717

471 [24] Kock, L. Raman spectroscopic studies of the underglaze pigments of porcelain shards of
472 archaeological origins. Chemistry Thesis, Pretoria: Faculty of Natural and Agricultural Sciences of the
473 University of Pretoria; 2009.

474 [25] Widjaja E, Hong Lim G, Lim Q, Mashadi A, Garland M. Pure component Raman spectral
475 reconstruction from glazed and unglazed Yuan, Ming and Qing shards: a combined Raman
476 microscopy and BTEM study. J Raman Spectrosc 2011; 42: 377-382. https://doi.org/10.1002/jrs.2721

477 [26] Carter E, Wood M, De Waal D, Edwards G. Porcelain shards from Portuguese wrecks: Raman
478 spectroscopic analysis of marine archaeological ceramics. Herit Sci 2017; 5: 17.
479 https://doi.org/10.1186/s40494-017-0130-9

480 [27] Bosi F, Halenius U, D'Ippolito V, Andreozzi G. Blue spinel crystals in the $MgAl_2O_4$-$CoAl_2O_4$ series:
481 Part II. Cation ordering over short-range and long-range scales. Am Miner 2012; 97: 1834-1840.
482 https://doi.org/10.2138/am.2012.4139

483 [28] Llusar M, Forés A, Badenes J, Calbo J, Tena M, Monrós G. Colour analysis of some cobalt-based
484 blue pigments. J Eur Ceram Soc 2011; 21: 1121-1130. https://doi.org/10.1016/S0955-2219(00)00295-
485 8

486 [29] Fernandez A, De Pablo L. Formation and the Color Development in Cobalt Spinel Pigments. Pigm
487 Resin Technol 2002; 31: 350-356. https://doi.org/10.1108/03699420210449043

488 [30] Cavalcante P, Dondi M, Guarini G, Raimondo M, Baldi G. Colour performance of ceramic nano-
489 pigments. Dyes Pigm 2009; 80: 226-232. https://doi.org/10.1016/j.dyepig.2008.07.004

490 [31] D'Ippolito V, Andreozzi G, Bosi F, Halenius U. Blue spinel crystals in the $MgAl_2O_4$-$CoAl_2O_4$ series:
491 Part I. Flux growth and chemical characterization. Am Miner 2012; 97: 1828-1833.
492 https://doi.org/10.2138/am.2012.4138

493 [32] Srisawad N, Chaitree W, Mekasuwandumrong O, Praserthdam P, Panpranot J. Formation of
494 $CoAl_2O_4$ Nanoparticles via Low-Temperature Solid-State Reaction of Fine Gibbsite and Cobalt
495 Precursor. J Nanomater 2012: 1. https://doi.org/10.1155/2012/108369

496 [33] Melo D, Cunha J, Fernandes J, Bernardi M, Mela M, Martinelli A. Evaluation of $CoAl_2O_4$ as
497 ceramic pigments. Mater Res Bull 2003; 38: 1559-1564. https://doi.org/10.1016/S0025-
498 5408(03)00136-3

499 [34] Zayat M, Levy D. Blue $CoAl_2O_4$ Particles Prepared by the Sol–Gel and Citrate–Gel Methods. Chem
500 Mater 2000; 12: 2763-2769. https://doi.org/10.1021/cm001061z

501 [35] Ahmed I, Shama S, Moustafa M, Dessouki H, Ali A. Synthesis and spectral characterization of
502 $Co_xMg_{1-x}Al_2O_4$ as new nano-coloring agent of ceramic pigment. Spectro Acta A 2009; 74: 665-672.
503 https://doi.org/10.1016/j.saa.2009.07.024

504 [36] Duan X, Pan M, Yu F, Yuan D. Synthesis, structure and optical properties of $CoAl_2O_4$ spinel
505 nanocrystals. J Alloys Compd 2011; 509: 1079-1083. https://doi.org/10.1016/j.jallcom.2010.09.199

506 [37] Salem S, Bondioli, F. Evaluation of green and blue cobalt aluminate spinels,
507 http://www.nanoparticles.ch/archive/2012_Salem_PO.pdf ; 2012 [accessed 20 December 2019]

508 [38] Deer W, Howie R, Zussman J. An introduction to the rock-forming minerals. 2nd edition. Harlow:
509 Longman Scientific & Technical; 1992.

510   [39] Torkian L, Daghighi M, Boorboor Z. Simple and Efficient Rout for Synthesis of Spinel
511   Nanopigments. J Chem 2013: ID 694531. https://doi.org/10.1155/2013/694531

512   [40] Khattab R, Sadek H, Gaber A. Synthesis of $Co_xMg_{1-x}Al_2O_4$ nanospinel pigments by microwave
513   combustion method. Ceram Int 2017; 43: 234-243. https://doi.org/10.1016/j.ceramint.2016.09.144

514   [41] Fahlman B. Materials Chemistry. Dordrecht: Springer; 2007.

515   [42] Möncke D, Papageorgiou M, Winterstein-Beckman A, Zacharias N. Roman glasses coloured by
516   dissolved transition metal ions: redox-reactions, optical spectroscopy and ligand field theory. J
517   Archaeol Sci 2014; 46: 23-36. https://doi.org/10.1016/j.jas.2014.03.007

518   [43] Green L, Hart A. Colour and chemical composition in ancient glass: An examination of some
519   Roman and Wealden glass by means of ultraviolet-visible-infra-red spectrometry and electron
520   microprobe analysis. J Archaeol 1987; 14: 271-282. https://doi.org/10.1002/jrs.5358